Article ID: 1006-8775(2022) 03-0308-18

Sensitivity Analysis of the Super Heavy Rainfall Event in Henan on 20 July (2021) Using ECMWF Ensemble Forecasts

HUANG Qi-jun (黄绮君)[1], GE Xu-yang (葛旭阳)[1], PENG Melinda (彭顺台)[2], DENG Zhong-ren (邓中仁)[1]
(1. Key laboratory of Meteorological Disaster of Ministry of Education, Joint International Research Laboratory of Climate and Environment Change, Collaborative Innovation Center on Forecast and Evaluation of Meteorological Disasters, Nanjing University of Information Science and Technology, Nanjing 210044 China;
2. University of Colorado, Colorado Spring, Colorado 80918 USA)

Abstract: An unprecedented heavy rainfall event occurred in Henan Province, China, during the period of 1200 UTC 19 -1200 UTC 20 July 2021 with a record of 522 mm accumulated rainfall. Zhengzhou, the capital city of Henan, received 201.9 mm of rainfall in just one hour on the day. In the present study, the sensitivity of this event to atmospheric variables is investigated using the ECMWF ensemble forecasts. The sensitivity analysis first indicates that a local Yellow-Huai River low vortex (YHV) in the southern part of Henan played a crucial role in this extreme event. Meanwhile, the western Pacific subtropical high (WPSH) was stronger than the long-term average and to the west of its climatological position. Moreover, the existence of a tropical cyclone (TC) In-Fa pushed into the peripheral of the WPSH and brought an enhanced easterly flow between the TC and WPSH channeling abundant moisture to inland China and feeding into the YHV. Members of the ECMWF ensemble are selected and grouped into the GOOD and the POOR groups based on their predicted maximum rainfall accumulations during the event. Some good members of ECMWF ensemble Prediction System (ECMWF-EPS) are able to capture good spatial distribution of the heavy rainfall, but still underpredict its extremity. The better prediction ability of these members comes from the better prediction of the evolution characteristics (i.e., intensity and location) of the YHV and TC In-Fa. When the YHV was moving westward to the south of Henan, a relatively strong southerly wind in the southwestern part of Henan converged with the easterly flow from the channel wind between In-Fa and WPSH. The convergence and accompanying ascending motion induced heavy precipitation.

Key words: ensemble forecast; extremely heavy rainfall; sensitivity analysis
CLC number: P458 **Document code:** A
Citation: HUANG Qi-jun, GE Xu-yang, PENG Melinda, et al. Sensitivity Analysis of the Super Heavy Rainfall Event in Henan on 20 July (2021) Using ECMWF Ensemble Forecasts [J]. Journal of Tropical Meteorology, 2022, 28(3): 308-325, https://doi.org/10.46267/j.1006-8775.2022.024

1 INTRODUCTION

Rainstorms often can cause serious disasters, such as flooding, landslides, and mountain torrents. Recently, a historical rainfall event hit Henan Province in central China during the period of 1200 UTC 19 -1200 UTC 20 July 2021 with 24-hour accumulation of 522 mm rainfall (Fig. 1). Zhengzhou, the capital city of Henan, received 201.9 mm of rainfall in just one hour on July 20, breaking the hourly record in China. This extreme precipitation event (named as "21.7" event hereafter) caused a death toll of 302, and a direct economic loss of over 100 billion RMB.

Previous studies pointed out that heavy rainfall events in China are often associated with frontal systems, typhoons, low-level vortices, or other weather events (Luo et al. [1]; Chen and Luo. [2]; Li et al. [3]). Meanwhile, a rainstorm can result from multi-scale interactions across meso-scale and large-scale synoptic systems (Chen and Li [5]; Houze et al. [6]; Houze [7]; Lau et al. [8]; Zhang et al. [9]; Iwasaki [10]; Luo et al. [11]; Luo and Chen [12]; Luo et al. [13]). During the "21.7" heavy rainfall event, several weather systems occurred in the East Asian region. For example, tropical cyclone In-Fa (2106) was formed on 18 UTC 17 July, located in the Northwest Pacific (132.5 °E, 22.2 °N). It has been well acknowledged that typhoon can contribute remote rainstorms by building up the heat and water vapor channels (Wang et al. [14]; Cong et al. [15]). The pathway of water vapor or atmospheric river is largely determined by the intensity and location of the tropical cyclone that leads to the heavy rainfall events (Wang et al. [14]; Wu et al. [16]).

Studies have shown that rainstorm forecasts are sensitive to initial uncertainties (Luo and Zhang [17]; Zhou and Cui [18]). As such, the ensemble technique, which contains perturbed states representing a variety of uncertainties, becomes more popular in operational

Submitted 2022-03-01; **Revised** 2022-05-15; **Accepted** 2022-08-15
Funding: National Natural Science Foundation of China (42175003, 42088101); Graduate Research and Innovation Projects of Jiangsu Province (KYCX22_1134)
Biography: HUANG Qi-jun, primarily undertaking research on tropical cyclone and mesoscale meteorology
Corresponding author: GE Xu-yang, e-mail: xuyang@nuist.edu.cn

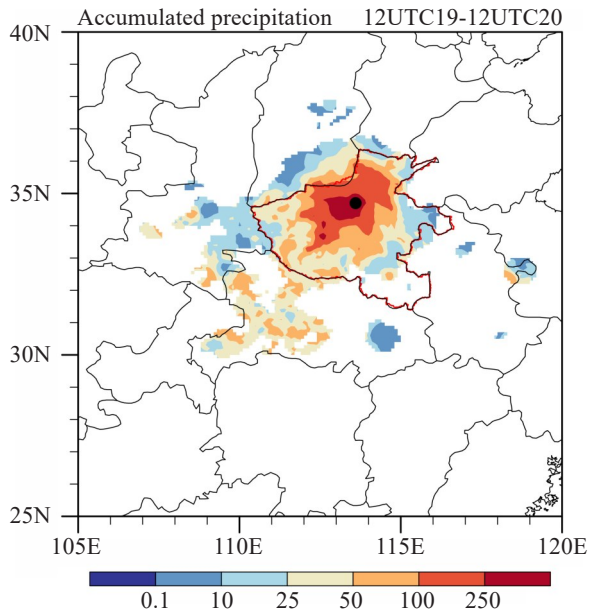

Figure 1. Observed 24-hour accumulated rainfall amount (units: mm) from 12 UTC 19 to 12 UTC 20 July (The black dot represents Zhengzhou City).

centers. The technique of ensemble-based sensitivity analysis (ESA hereafter; Ancell and Hakim [19]; Hakim and Torn [20]) uses an ensemble of equally likely analyses and forecasts to compute statistical estimates of initial condition sensitivity and observation impact. This method has been used to understand the underlying physical mechanism of weather events such as extratropical cyclones and tropical cyclones (Torn and Hakim [21]; Brown and Hakim [22]), the blocking high pressure (Matsueda et al. [23]; Quandt [24]), the easterly wave (Torn [25]), the strong convection (Hill et al. [26]; Limpert and Houston [27]), and rainstorms (Yu and Meng [28]; Du and Chen [29]; Wu et al. [30]).

It usually requires that both dynamical and thermodynamical conditions be conducive to heavy rainfall development. Due to the extreme precipitation, it is important to understand the underlying dynamical and thermodynamical processes associated with the "21.7" event. Numerous recent observational and numerical studies focused on this extreme rainstorm. It is suggested that this event was closely related to the multi-scale interactions among TC In-Fa, upper-level mid-latitude weather systems, and the subtropical high (Ran et al. [31]; Shi et al. [32]). By using the FY-4A stationary satellite imager data and ground-based weather radar data, Sun et al. found that active convection in a transport zone of water vapor [33]. Zhang et al. suggested that the abnormality of atmospheric circulations and the environmental physical quantities could indicate extreme rainstorms [34]. Due to limited model resolution and time intervals, global ensemble forecast systems lack the capability to solve some crucial issues especially on the mesoscale convective system. The ensemble-based sensitivity analysis (ESA) is applied to evaluate the sensitivity of the forecast to different state variables. In the first step, the ESA is used to explore some possible synoptic scale systems that potentially impact this local extreme event. In the next step, sensitivity experiments with cloud-resolving regional model will be conducted to test these possible candidates. This is our motivation in this study. Through high-resolution simulations, we attempt to identify weather systems contributing to the extreme heavy rainfall event and compare the influence of them on the event.

The rest of the paper is organized as follows. In Section 2, the ECMWF-EPS for the "21.7" event is examined. In Section 3, the ensemble-based sensitivity analysis is computed to evaluate the sensitivity of the forecast to different state variables. Section 4 presents some physical understanding of the event by comparing the good and poor ensemble predictions on different parameters. The discussion and conclusions are given in Section 5.

2 ENSEMBLE FORECASTS OF THE RAINFALL EVENT

In this study, 50 members from the ECMWF ensemble forecast, initialized at 0000 UTC 17 July with a total of 120 h of integration, are utilized. The horizontal grid resolution of the ensemble forecast data is 0.5 °×0.5 ° with 6 layers from 1000-hPa to 200-hPa, and outputs at a 6-hour interval. Fig. 2 shows the 24-hour accumulated precipitation in each member from 12 UTC 19 to 12 UTC 20 July. Notice that there is a large spread among the members in terms of both the location and magnitude of the maximum rainfall. All the forecasts underestimated the extreme of the rainfall compared to the observation (Fig. 1). Furthermore, the forecasted location in most of the members show some westward bias. Among them, 21 members were selected subjectively and divided into two groups. The Good group consists of 10 members (marked with red boxes) with the maximum accumulated precipitation greater than 100 mm. There are 11 members in the "POOR" group with the maximum accumulated precipitation less than 50 mm (blue boxes).

The average 24-hour accumulated precipitation between two groups are compared in Fig. 3. As expected, the GOOD group has a better forecast performance on the rainfall than the POOR group. Specifically, in the GOOD group, the average maximum accumulated precipitation was about 110 mm, and was located closer to Zhengzhou. The average maximum accumulated precipitation of the POOR members in Henan Province was about 45 mm, and the precipitation area was more scattered.

3 ENSEMBLE SENSITIVITY ANALYSIS

The ensemble forecasts show a pronounced variability in the rainfall prediction for the "21.7" event

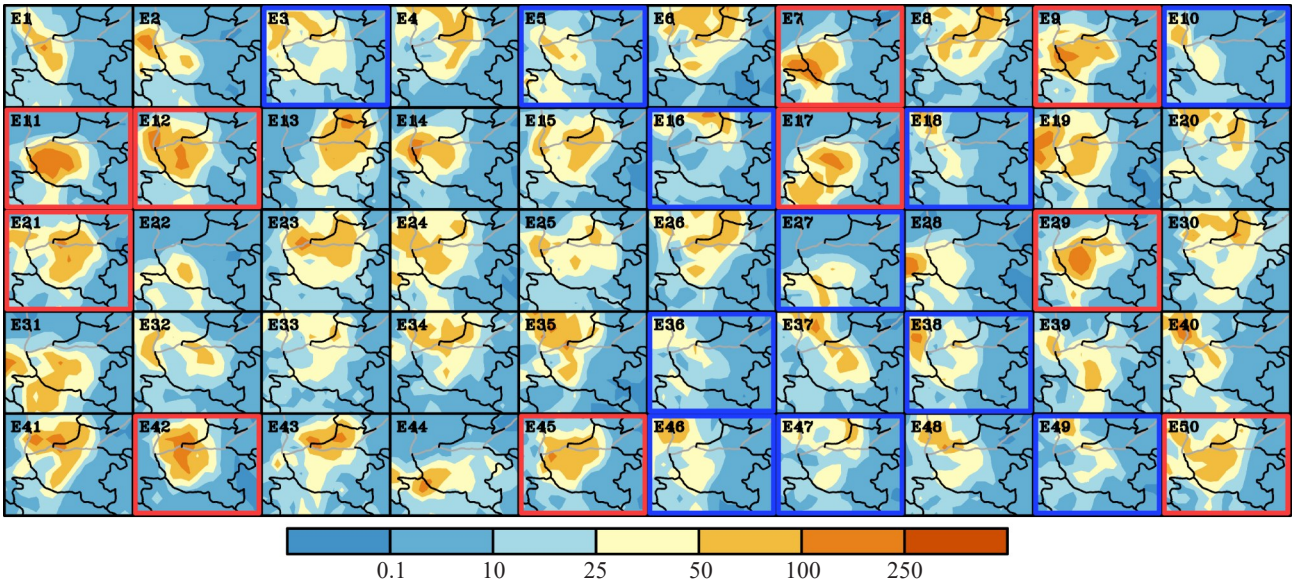

Figure 2. 24-hour accumulated precipitation of the ECMWF ensemble members from 12 UTC 19 to 12 UTC 20 July. The red (blue) boxes indicate the selected members in GOOD (POOR) group, respectively.

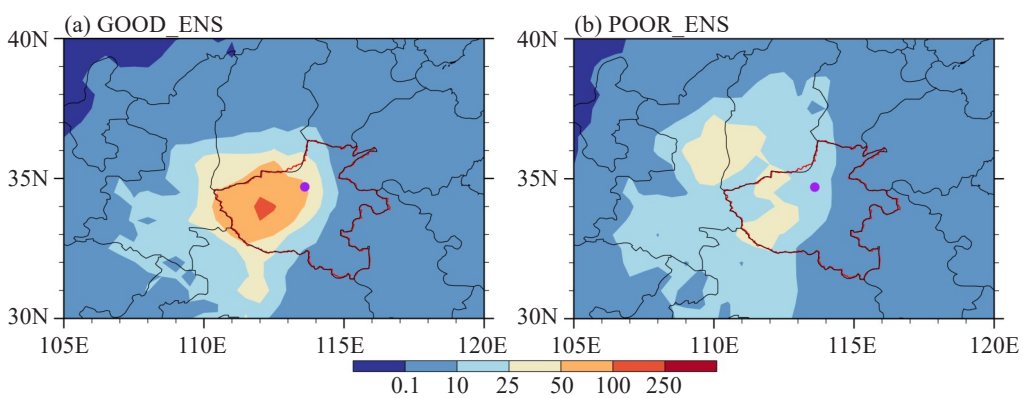

Figure 3. Averaged 24-hour accumulated precipitation of (a) the 10 good members and (b) the 11 poor members from 12 UTC 19 to 12 UTC 20 July (The purple dot represents Zhengzhou).

(Fig. 2). Here, the ESA is applied to explore possible dynamical and thermodynamical processes accounting for this extreme case. Following Torn and Hakim, the ensemble sensitivity is evaluated from an *M*-member ensemble via [35]

$$S = \frac{\partial J}{\partial x_i} = \frac{\mathrm{cov}(J, x_i)}{\mathrm{var}(x_i)} \quad (1)$$

where J is $1 \times M$ ensemble estimates of the forecast metric and x_i is the ith state variable from ensemble data, cov is the covariance between J and x_i, and var is the variance. Equation (1) represents a linear relationship between the forecast metric and each state variable. In general, this sensitivity calculation reveals the sensitivity of a subject metric to each model variable. In this study, the forecast metric is the 24-h accumulated precipitations of the ECMWF-EPS from 1200 UTC 19 to 1200UTC 20 July.

Figure 4a presents the mean 850-hPa circulation for the 50 members of the ensemble on 12 UTC 18 July. A tropical cyclone, Typhoon In-Fa (2106), was located in the northwest Pacific basin and a low vortex was located at the southern part of Henan Province in central China (usually known as Yellow-Huai River Vortex; YHV, Yang et al. [36]). The Western Pacific subtropical high (WPSH), highlighted by the 1520 geopotential meter (gpm) contour, was located at the mid-latitude (about 38 °N). Fig. 4b presents the ensemble-mean of the 500-hPa circulation and geopotential height field. There existed a continental high-pressure system (CH hereafter) to the northwest of the YHV, shown more clearly on the 500 hPa level than on 850 hPa. There was a deeper mid-latitude westerly trough between CH and WPSH. Similarly, the deeper westerly trough has impact on WPSH moving to north. Fig. 4c displays the sensitivity of the 24h accumulated rainfall amount to the 850-hPa geopotential height field by the forecasts of the 50 ensemble members from ECMWF-EPS. The positive sensitivity reflects a positive correlation between two entities while a negative sensitivity indicates the

opposite. Generally, the larger the differences among the ensemble members, the larger the sensitivity value. The large areas of sensitivity indicate great differences in the predictions of the position and intensity of TC, YHV, and WPSH among 50 ensemble members. Not surprisingly, if the YHV is predicted to be at the southern part of Henan Province, it will be of more contribution to the rain event over Henan when a positive sensitivity area is located to the northern part of Henan. The sensitivity associated with TC In-Fa (2016) presents similar indication as with the YHV, with the positive sensitive area to the northwest of the TC. Since the WPSH covers the largest area in the domain of interest, the associated sensitivity area is also the largest. Focusing on the center of WPSH, the broad area of negative area suggests that if the WPSH is predicted to be more to the southeast, it does not favor the heavy rainfall event in central China. Furthermore, an area with positive value occurs to the north of the ensemble-mean WPSH, indicating ensemble members having an anomalously northward shift of the WPSH is more conducive to the rainfall event than other members. This analysis indicates that WPSH moving to the north is conducive to the heavy rainfall in the area of interest. Fig. 4d for the sensitivity analysis on 500-hPa shows similar features as on the 850-hPa with a more pronounced sensitivity associated with the mid-latitude trough between CH and WPSH.

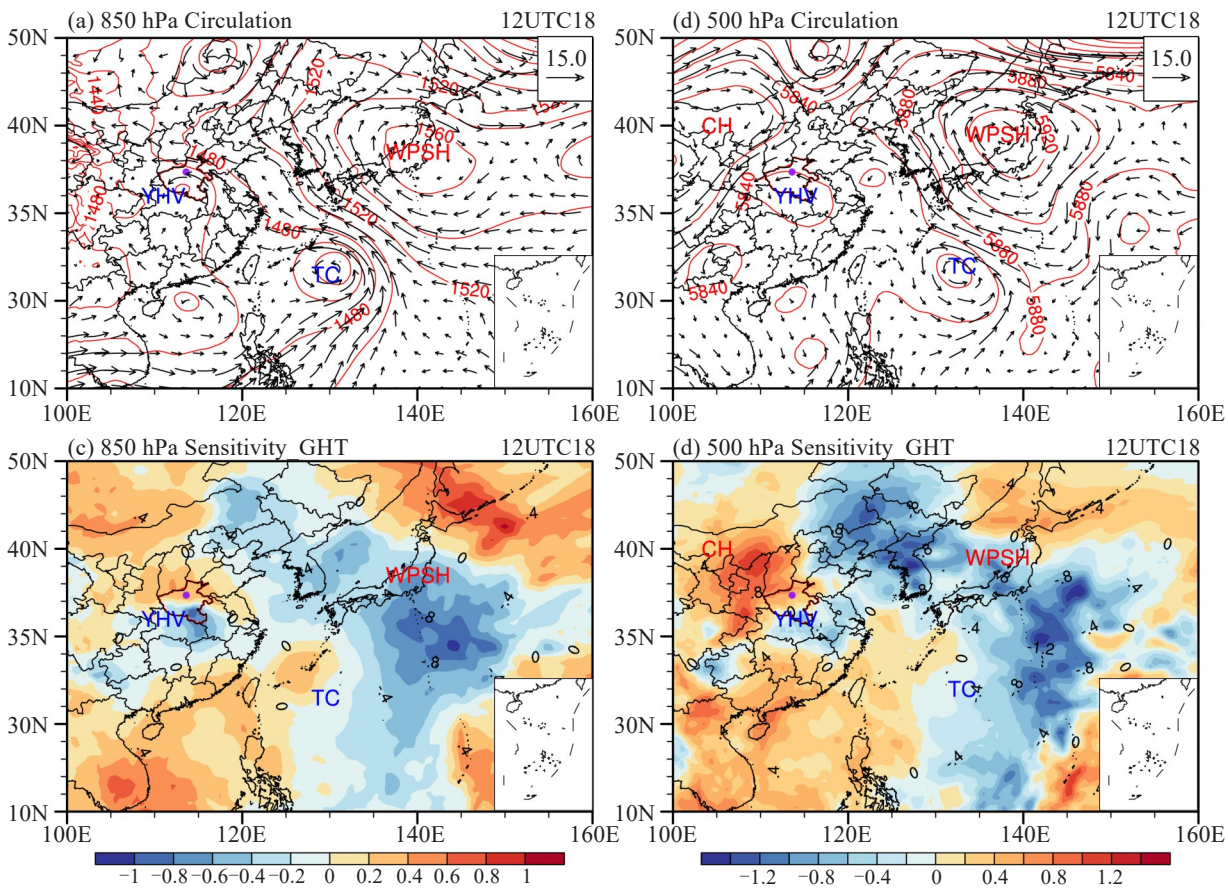

Figure 4. The ensemble-mean circulation (m s^{-1}), geopotential height field (m), and the sensitivity (mm gpm^{-1}) of the forecasted 24-hour accumulated precipitation (mm) to geopotential height (gpm) at 12 UTC 18 July by the 50 ensemble members from ECMWF-EPS. (a) on 850-hPa; (b) on 500-hPa (red contour: the geopotential height field); (c) the sensitivity to the 850-hPa geopotential height; (d) the sensitivity to the 500-hPa geopotential height.

In general, the stronger TC and YHV, the greater the rainfall amount is. In the CH region, the sensitivity is more pronounced at 500-hPa than on 850-hPa. The associated positive value reflects an enhanced high-pressure system and is positive for the heavy rain event in Henan. There is a big negative value associated with the westerly trough between the WPSH region and CH region in the mid-latitude. The negative value in the mid-latitude implies that the deeper westerly trough is favorable for the rain event. The sensitivity analysis for the rainfall event suggests major influences from the YHV in the south of Henan, the WPSH, and TC In-Fa. Therefore, we will take a closer examination on these systems in the following sections.

In summary, the ESA indicates the weather systems which are different in the ensemble prediction from ECMWF-EPS that have potential impacts on the "21.7" extreme rainfall event. The sensitivity analysis suggests that the combined activities of the YHV, the TC and the WPSH induced the perfect storm scenario for the heavy

rainfall event. These entities will be further investigated. Moreover, the sensitivity of the rainfall amount to the moisture field will be discussed in Section 4.3.

4 DYNAMICAL AND PHYSICAL PROCESSES

Guided by the ESA sensitivity analysis, we examine entities showing large sensitivity and investigate the physical and dynamical processes associated with the extreme rain event.

4.1 *Yellow-Huai River vortex*

The low-level cyclonic vortex located between the Yellow River and Huai River plays an important role in many rainstorm events in North China (Luo et al. [1]; Chen and Luo [2]; Li et al. [3]). It has been well acknowledged that the movement of the low vortex is largely affected by the mid-latitude westerly trough and WPSH. Specifically, Yang et al. pointed out the critical role of YHV in the heavy rainfall events, particularly in Henan[36]. The ESA in Fig.4 c and d also indicate that a large sensitivity is located in the YHV region, implying a potential linkage between YHV and the "21.7" rainfall event. This motivates us to examine the evolution of this entity in the ensemble forecast.

To better illustrate the YHV circulation for the GOOD and POOR group, a perturbation weather map (Qian et al. [37]) is used, which is obtained by subtracting the average of each group from the climatologically daily mean (Fig. 5). Shown is a cyclonic circulation associated with YHV in both groups, which moves westward and decays gradually during the period of interest. This entity is located on the southeast side of Henan on 18 July, one day into the forecast, and anomalous easterlies are prevailing around Zhengzhou City. The GOOD and POOR group show only little differences between them (Fig. 5a, b and c). A marked difference in the strength and location of YHV evolved between the two groups during the following 48 hours. The vortex maintains its structure in GOOD, whereas it is less organized in POOR. In reality, on 20 July, a relatively stronger southerly exists at the eastern flank of vortex center, which encounters with the easterly flow from the ocean and thus results in a great convergence in the adjacent of Zhengzhou City (not shown). In contrast, in POOR, the southerly flow is much weaker due to the weakening of the vortex. There is a prevailing southeasterly flow associated with the YHV and thus no significant convergence is generated between the YHV and the flow from the ocean.

To further demonstrate the differences of the forecasted YHV in the ensemble, the vertical structure of the vorticity across the center along 34° N is compared between the two groups (Fig. 6). On 18 July, both groups have a clear low-level vortex with a deep vertical structure penetrating upward to about 300-hPa. At this

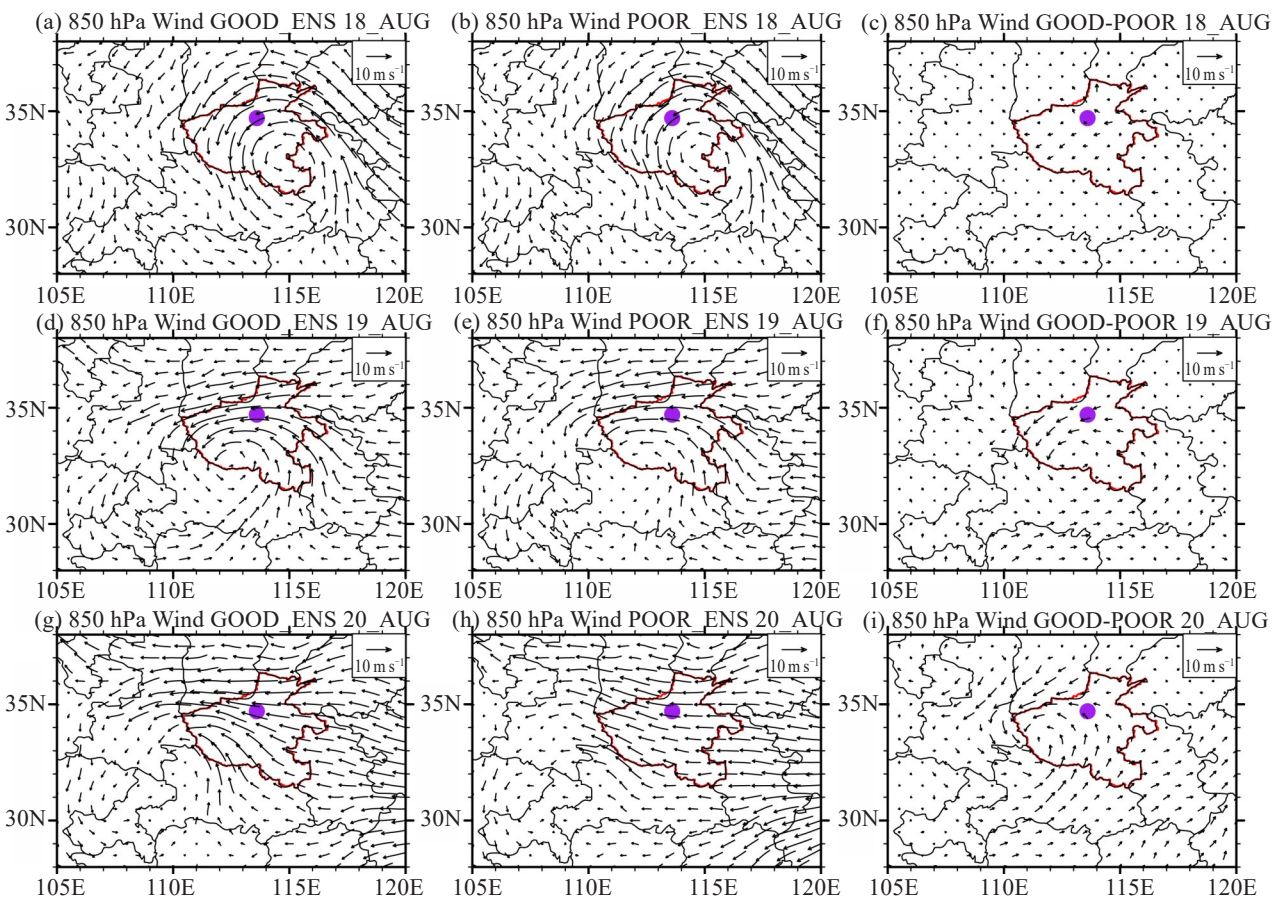

Figure 5. The time evolution of the averaged circulation which is obtained by subtracting the average of each group from the climatologically daily mean of the two groups on 850-hPa. (a, d, g) the 10 good members; (b, e, h) the 11 poor members; (c, f, i) the difference between the good and poor members. (The purple dot represents Zhengzhou).

moment, the vortex in GOOD is more intense compared with that in POOR. Thereafter, this low vortex moves westward and gradually weakens. The difference between the two groups becomes significant on July 20 in terms of its location and intensity. For instance, the entity is located at 111° E, and the vertical structure remains in GOOD, though weakened. The possible processes accounting for the weakening of YHV are not clear yet, and need further studies. Nevertheless, the vortex has nearly dissipated in POOR, especially at low levels.

The YHV is affected by both the rotating effect and the deformation effect. And the different developments of the YHV implies different dynamical effects. To investigate possible dynamical effects on YHV, the Okubo-Weiss parameter (OW) is computed, which distinguishes the rotating effect and the deformation effect (Okubo [38]; Weiss [39]). The OW is defined as

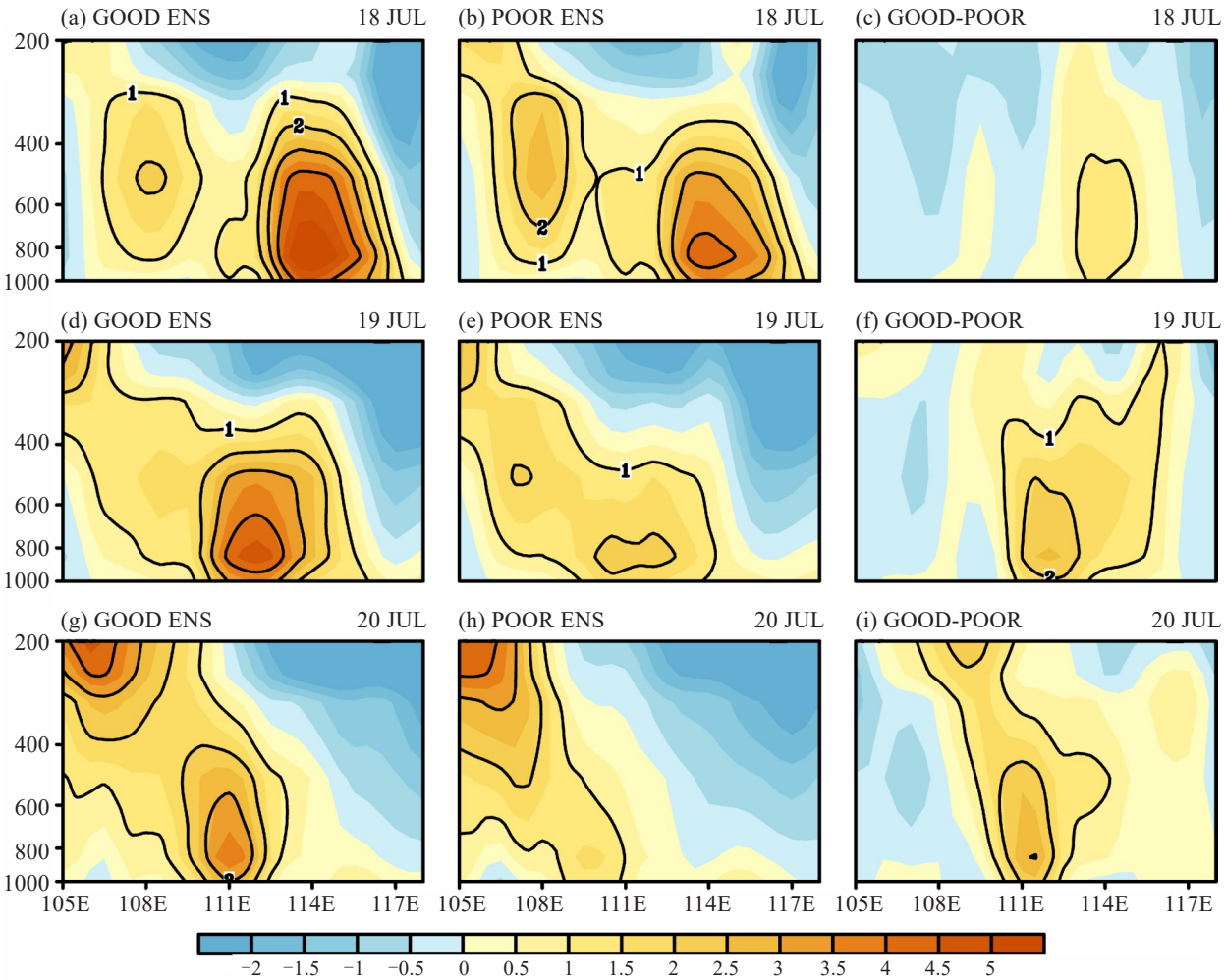

Figure 6. The vertical-longitude cross-section of the averaged relative vorticity (1×10^{-5}, unit: s^{-1}) of the low vortex along 34 °N for (a, d, g) GOOD and (b, e, h) POOR group, respectively; (c, f, i) panels represent the difference in between.

$$\mathrm{OW} = \zeta^2 - S_1^2 - S_2^2, \tag{2}$$

where $\zeta = \frac{\partial v}{\partial x} - \frac{\partial u}{\partial y}$ is the vorticity, $S_1 = \frac{\partial u}{\partial x} - \frac{\partial v}{\partial y}$ is the tensile deformation, $S_2 = \frac{\partial v}{\partial x} + \frac{\partial u}{\partial y}$ is the shear deformation, and u and v are zonal and meridional speed. Generally, the stronger the vortex, the greater the positive OW, which is conductive to the convection development. Conversely, once the deformation is dominant, it may inhibit the development of convection.

Figure 7 compares the 850-hPa OW for the two groups averaged from 12 UTC 19 to 12 UTC 20 July. Not surprisingly, a salient difference of the OW distribution occurs between the GOOD and POOR groups. A positive value in the southwest of Henan corresponds to the position of the YHV center in the GOOD group, indicating the rotating effect is favorable for the cyclonic development. Meanwhile, the negative OW over northern Henan indicating the deformation effect there is greater than the rotating effect and is detrimental to the YHV development. In general, the large OW areas in the POOR group (Fig. 7b), including both the positive and negative OW, are outside the actual YHV location, but correspond to the displaced YHV in the POOR group (Fig. 5). Overall, the OW diagnostics indicates that the development of YHV corresponds well with the dynamic processes in the two groups.

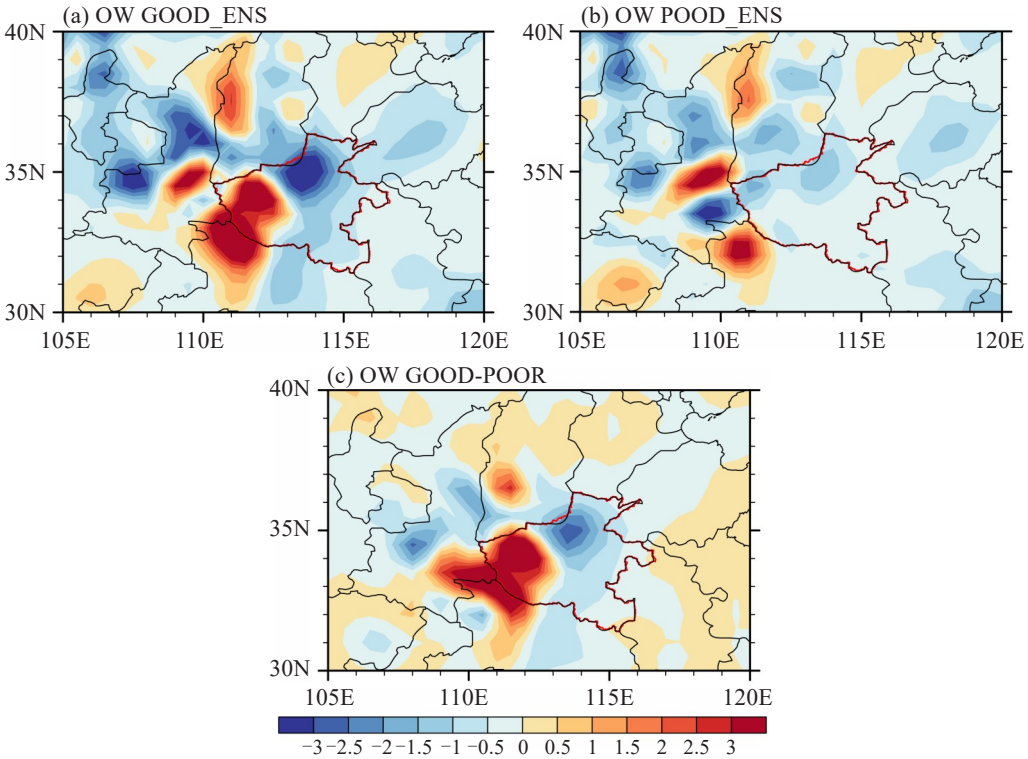

Figure 7. Time averaged 850-hPa OW index (1×10^{-9}, units: s^{-2}) for the two groups from 12 UTC 19 July to 12 UTC 20 July for (a) GOOD and (b) POOR group, respectively; (c) the difference between the two groups.

Next, we look at the upper-level dynamical processes. In general, the low-level (upper-level) convergence (divergence) promotes upward motions. To evaluate the upper-level influences, the residual of the Nonlinear Balance Equation (ΔNBE; Zhang et al. [40]) is calculated, which is defined as:

$$\Delta\mathrm{NBE} = 2J(u,v) + f\zeta - \nabla^2\Phi - \beta u, \qquad (3)$$

where the Jacobian operator $J(u,v) = (\partial u/\partial x \cdot \partial v/\partial y) - (\partial v/\partial x \cdot \partial u/\partial y)$, f is the Coriolis parameter, ζ is the relative vorticity, Φ is the geopotential height, ∇^2 is the 2-dimensional Laplace Operator, and $\beta = \partial f/\partial y$. This term reflects the tendency of divergent term, which is mainly ascribed to the large-scale dynamical imbalances. Dynamically, the larger the positive value of ΔNBE at higher levels, the stronger tendency of divergence. Fig. 8 presents the 200-hPa ΔNBE in the two groups at three different snapshots. Basically, during the period of interest, there are positive values of the ΔNBE in the western part of Henan in both groups. The value of ΔNBE in the GOOD group is significantly stronger than its counterpart in POOR,

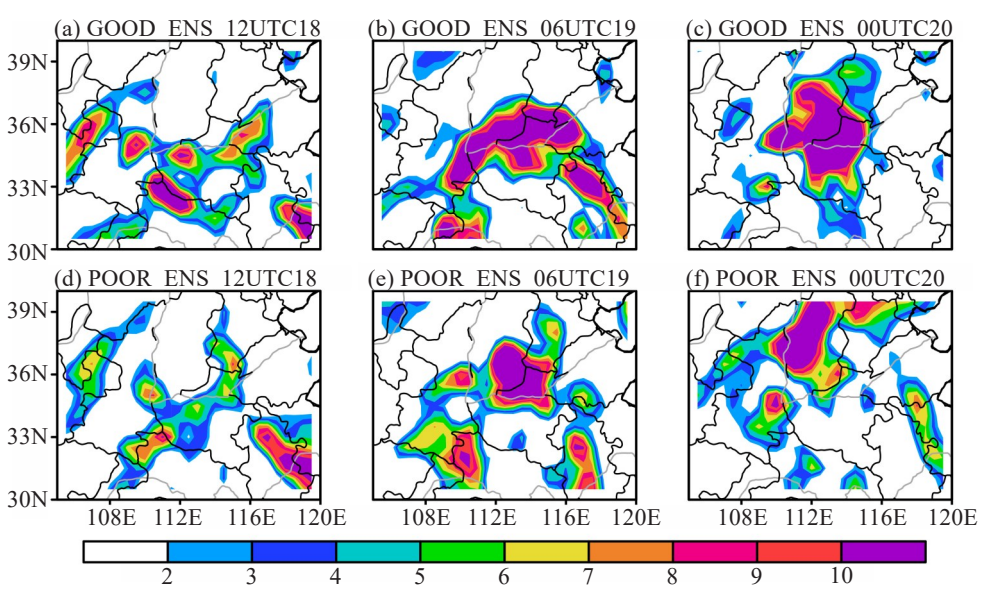

Figure 8. The ΔNBE (units: 1×10^{-5} s^{-2}) for the two groups on 200-hPa at 12 UTC 18, 06 UTC 19 and 00 UTC 20 July, respectively.

indicating a stronger upper-level divergence tendency. The area with positive ΔNBE moves northwestward over time, which is also consistent with the westward migration of YHV. Of particular interest is that Fig. 8f has a very similar pattern of the OW in the southwest of Henan in the POOR (Fig. 7b), indicating a dynamic consistency between them. Zhang et al. showed that the residual of the NBE contains sufficient information required to assess flow imbalance [40]. Under some circumstances, the region with pronounced ΔNBE likely reflects the source region of the gravity waves triggering the convection (Koch and Dorian [41]).

Figure 9 compares the simulated surface winds field at 10-m altitude and the associated divergence field. It is obvious that, in GOOD, there is a strong northeasterly (southerly) wind to the north (south) side of the target area. As a result, a pronounced surface convergence is evident in GOOD, implying a stronger lower-level dynamical lifting for convective initiation. The stronger low-level dynamical lifting is conductive to the development of YHV on 850-hPa (Fig. 5). The GOOD and POOR groups have similar wild fields on 18 July. However, the surface convergence weakened due to the weaker southerly wind in POOR group during the period of interest in the next 48h. In short, the results suggest that the surface convergence will affect the development of YHV by the low-level dynamical lifting and thus eventually affect the heavy rainfall.

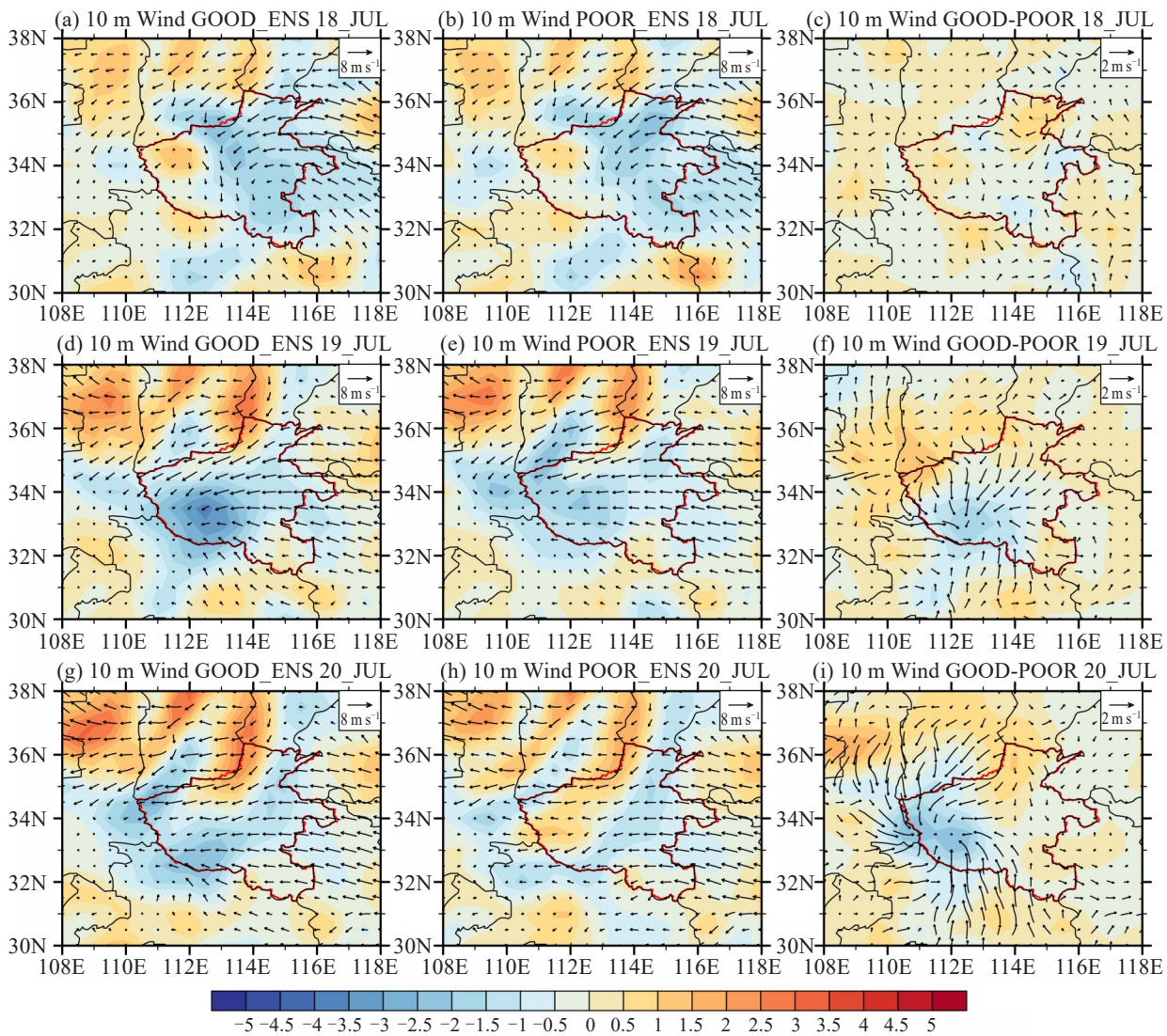

Figure 9. Time evolution of the simulated surface winds (m s^{-1}) field at 10-m altitude and the associated divergence field (1×10^{-5}; units: s^{-1}) for the two groups, (a, d, g) the 10 good members; (b, e, h) the 11 poor members; (c, f, i) the difference between good and poor members.

4.2 *Role of WPSH*

Since the WPSH occupies most area in the domain of interest and the sensitivity analysis also shows large regions of sensitivity, it deserves more attention. There are some differences between the WPSH on July, 2021 and the climatological WPSH. The climatological ridge of WPSH is located at around 30 °N and the western edge of the WPSH is located roughly at 140 °E (Fig.

10a). Without other synoptic anomalies, Henan would be mainly controlled by the climatological southerly wind flow on the west side of the WPSH. On 11 July, 2021, the ridge of WPSH was mainly located at about 29 °N, which was similar to the climatological field (Fig. 10b). However, the intensity of WPSH was stronger and the western edge of it extended to the west of the climatological WPSH. Figs. 10c and d show that on 15 July, a tropical depression (TD) was on the south side of the WPSH, and the TD developed into a TC on 18 July. The occurrence of TC In-Fa to the south of the WPSH pushed the WPSH to the north. A strong pressure gradient thus built up between TC and WPSH. The convergence of the anticyclonic flow from the WPSH and the cyclonic flow from In-Fa induced strong southeasterly flow toward the inland of China. The channel wind between the TC and WPSH brought large warm moisture from the ocean into northern China, fed into the YHV. Meanwhile, the persistent and strong WPSH blocked the TC from moving to the north and continuously supported the ample water vapor supply.

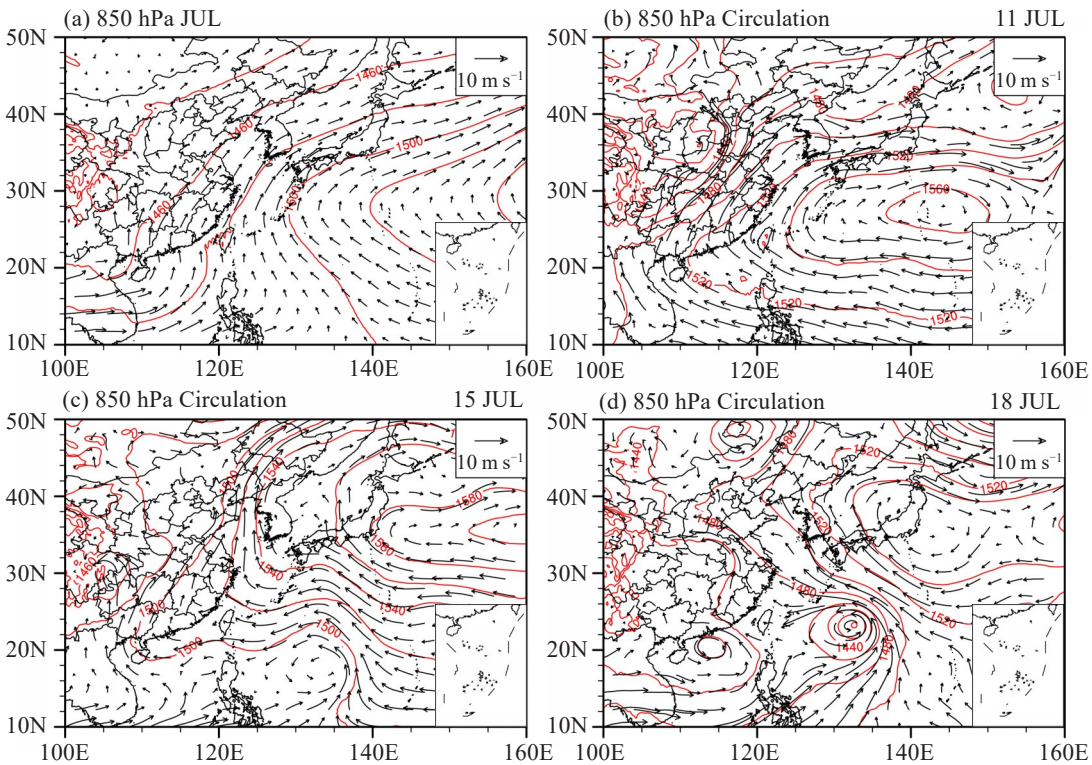

Figure 10. The circulation (units: m s^{-1}), and geopotential height field (m) on 850-hPa. (a) The climatological field by using ERA5 reanalysis data on July from 2011−2021; by using reanalysis data (b) on 11 July, 2021; (c) on 15 July, 2021; (d) on 18 July, 2021.

The result above suggests that the position of WPSH will affect the rainfall event. To further examine the differences of the forecasted WPSH in the ensemble, the geopotential height field is compared between the two groups in Fig. 11. The WPSH center was located at about 40 °N in both groups during the period of interest. And the WPSH moved to the west and north from 18 to 19 July. Since the WPSH covers the largest area, there are some differences of the intensity of WPSH between the two groups. The sensitivity to the geopotential height indicates that the WPSH moving to the north is conducive to the rainfall event (Fig.4c, d). The position of WPSH has effect on the rainfall prediction. However, the predicted WPSH is similar in both groups. Compared with the ERA5 reanalysis data (not shown), there is little difference between GOOD and POOR groups. This feature reflects, in general, GOOD and POOR groups have similar forecasts for the WPSH. We will show that the prediction of TC In-Fa plays a more critical role for the heavy rainfall event.

4.3 *Role of TC In-Fa*

Tropical cyclone can contribute to remote rainstorms by transporting heat and water vapor to the rainstorm area (Wang et al.[14]; Cong et al.[15]). In other incidents, typhoons acted as a strong source of disturbance that can disperse energy to the midlatitudes and lead to the convection (Xu et al.[42]; Lu et al.[43]). As aforementioned, the column integrated vapor transport (IVT; the detail discussion is in Section 4.5) pathway is closely associated with TC In-Fa. This motivates us to examine further the role of TC in the development of this extreme rainfall event. By taking the TC intensity (represented by the central minimum sea level pressure; CMSLP) as the predictor, we calculate the correlations between it and the low-level circulation, 500-hPa geopotential height, IVT, and the precipitation amount

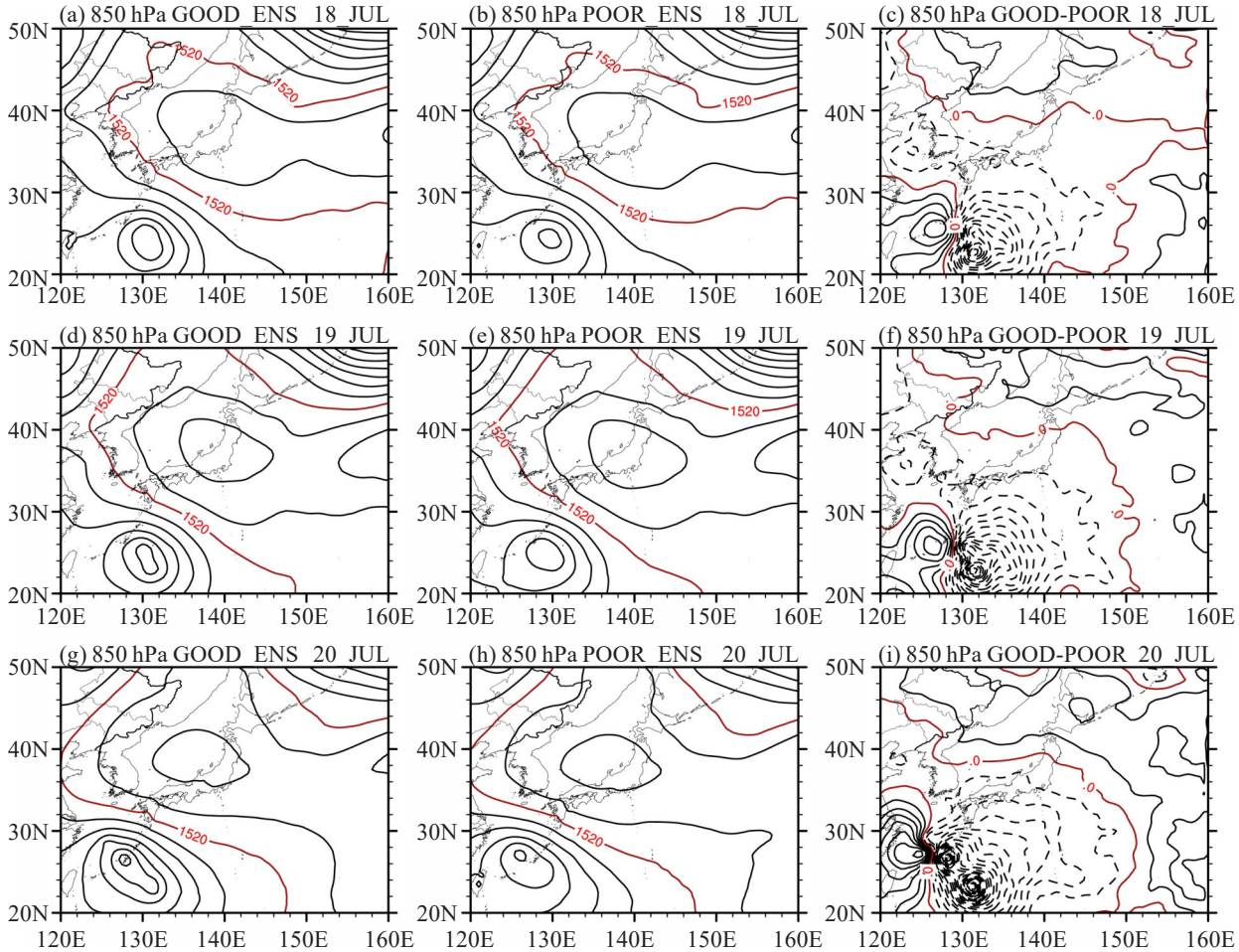

Figure 11. Time evolution of the averaged geopotential height of the two groups on 850-hPa. (a, d, g) the 10 good members; (b, e, h) the 11 poor members; (c, f, i) the difference between good and poor members.

using the ECWMF-EPS (Fig. 12). The correlation coefficient is multiplied by −1 . The 850 hPa wind is dominated by the TC circulation (Fig. 12a). The stronger the TC intensity, the stronger 500-hPa WPSH to the north as the TC pushes northward into the WPSH (Fig. 12b). Consequently, this pattern favors an enhancement of the easterly flow in between, and transports the abundant water vapor supply westward to Henan (Fig. 12c). Therefore, the positive correlation in the south of Henan indicates that the exist of the strong TC to the south of WPSH plays an important role in the heavy rainfall in the south of Henan (Fig. 12d). The small positive correlation coefficient between the TC and rainfall indicates little spread in TC intensity.

Figure 13 compares the positions and the intensities of TC In-Fa and the rainfall amount between the two groups from 17 to 19 July. The location of the TC and the averaged location of it (represented by the symbol of star) are given in the left panel (Fig.13 a, c, and e). The red (blue) dots represent the members in GOOD (POOR) group, respectively. The black stars are the TC locations from the best track dataset. During the period of the interest, the mean position of the TC in POOR group is located more to the west compared to that of GOOD, indicating a faster moving speed in the former. However, the observed TC is located more eastward than those members. The right panels of Fig. 13 show the boxplots of the intensities of the TC-vortices in the two groups. The black line represents the observed TC intensity. During the period of interest, the observed TC intensity is stronger. Initially, there is little difference between two groups. The intensity and position of TCs of the two groups diverged with time. Specifically, on 19 July, the mean intensity is about 992 (997) hPa in GOOD (POOR), respectively. The predicted TCs in the GOOD group are little stronger than those in the POOR group. As shown before, there is a small positive correlation between TC intensity and rainfall amount (Fig. 12 d). Moreover, the location of the TC also has an effect on the rainfall amount in Henan. The faster moving TC with a weak intensity in the POOR group corresponds to the weaker rainfall amount in Henan than in the GOOD group (Fig.13 g, h). Due to the weaker TC moving faster in the POOR group, the weaker channel wind between the TC and the WPSH brings less moisture into the YHV. The main rainfall amount occurred near the TC in POOR group. In short, the results above point out that the influences of the location

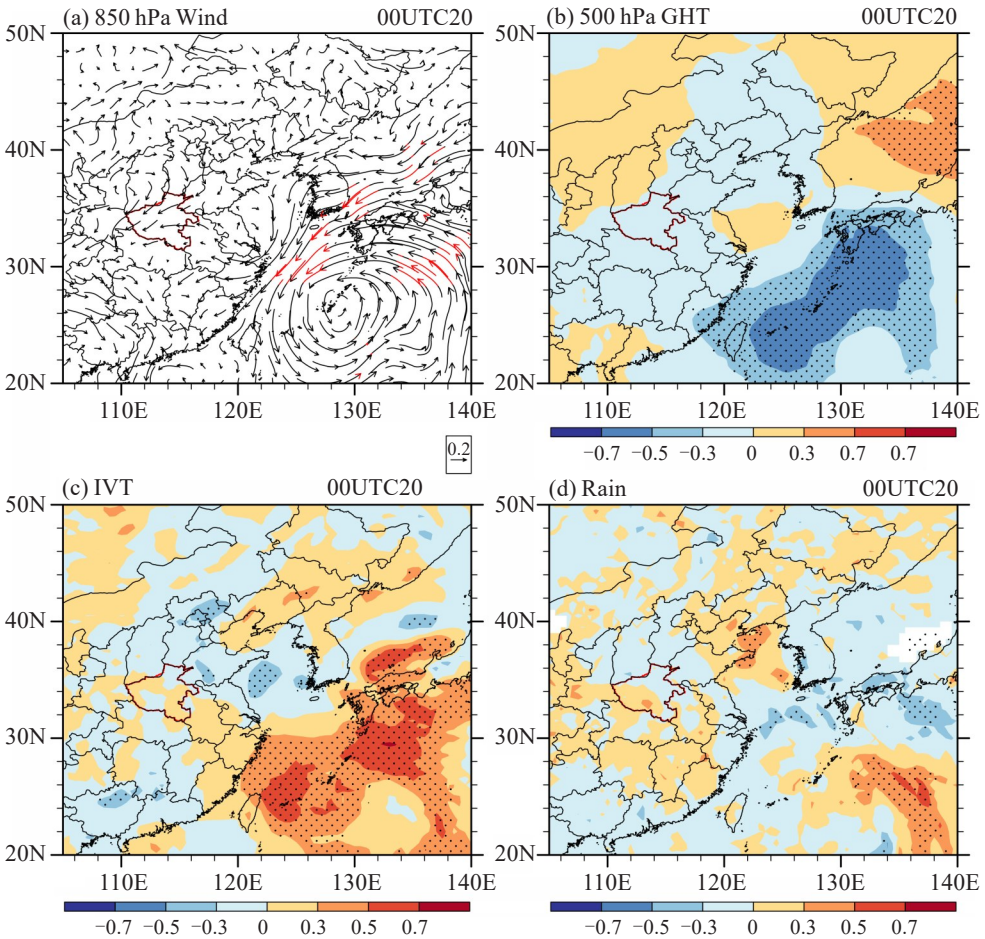

Figure 12. The correlation between typhoon intensity and wind circulation, geopotential height, IVT, and precipitation by the 50 ensemble members from ECMWF-EPS on 00 UTC 20 July. (Areas that pass the 95% significance test are represented by red vectors in (a) and dots in (b, c, d)).

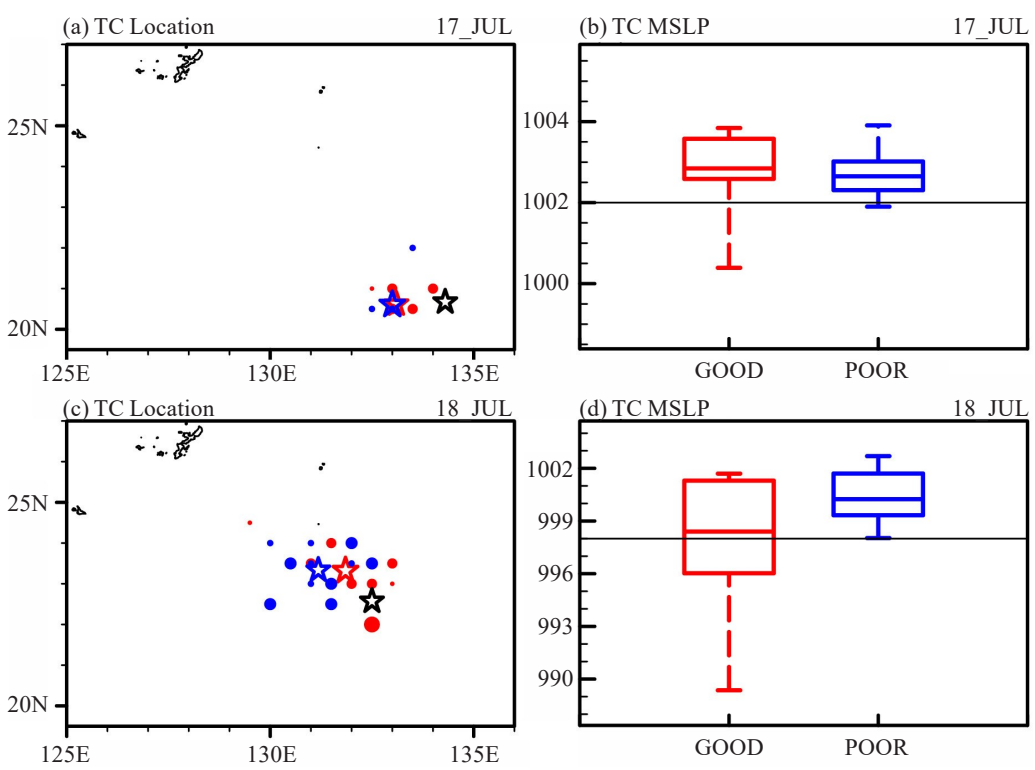

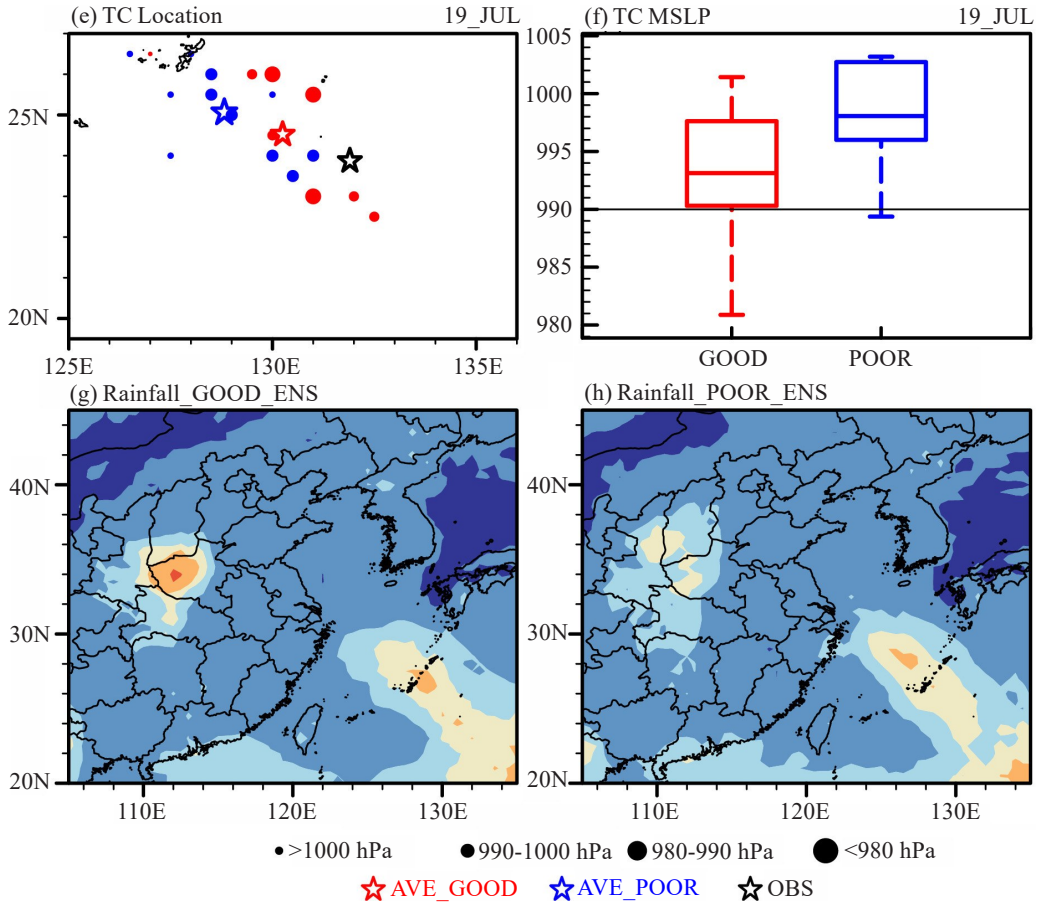

Figure 13. Left panels (a, c, e): the positions of the TCs from 17 July to 19 July. (Red dots represent 10 members in the GOOD group; blue dots represent 11 members in the POOR group; red star represents the averaged position of the GOOD group; blue star represents the averaged position of the POOR group; black star represents the TC best track; the sizes of the dots represent the intensities of the TCs). Right panels (b, d, f): the boxplots of the intensities of the TCs in the two groups from 17 July to 19 July. Averaged 24-hour accumulated precipitation of (g) the GOOD group and (h) the POOR group from 12 UTC 19 to 12 UTC 20 July. (Box with compartment is formed by the lower quartile, the median, and the upper quartile. The extension line is between the minimum value and the maximum value. The black lines in the right panel are the observational TC intensity).

and intensity of TC In-Fa on the heavy rainfall event.

4.4 *PV perspective*

It is well understood that potential vorticity (PV) is a physical quantity that can comprehensively characterize the thermodynamical and dynamical structure (Rossby [44]; Ertel [45]). With this regard, the PV field is examined to illustrate the possible differences between the two groups. Three snapshots of the 500-hPa PV are shown in Fig. 14. At 1200 UTC 18 July, there exists a mid-latitude westerly trough between WPSH and CH that affects the rainfall event (Fig. 4b, d). This suggests that the stronger high-pressure systems likely induce a deeper low-pressure trough in between and thus a greater PV. The mid-latitude westerly trough region is characterized by a high PV band structure extending southwestward. During the period, some scattered region with higher PV start to emanate around Henan, and the value of scattered PV is higher in the GOOD group than that in the POOR group.

Figure 15 depicts the vertical cross sections of the PV along the lines depicted in Fig. 14. In the early stage (i. e., at 12 UTC 18 July), there is a mid-tropospheric positive PV anomaly at (33.6 °N, 133.5 °E). Although there are some similarities in the vertical distribution of the two groups, the magnitude of PV in the GOOD group is greater than its counterpart in the POOR. This positive PV anomaly moves westward in the next 24h in both groups, agreeing well with the westward migration of the YHV. In the next 24 hours, in the GOOD group, another upper-level PV source centered at (35.7 ° N, 108.4 °E) starts to develop downward, connecting with the one with the westward movement. Meanwhile, the low-level vorticity center has moved too fast and is connected to the upper-level trough with the loss of its own signature by 1200 UTC 20 August in the POOR group (Fig. 15f).

4.5 *Water vapor transport*

The supply of water vapor plays an important role in the occurrence and development of extreme rainfall event (Doswell et al. [46]). In the present study, the IVT (Zhu and Newell [47]) is calculated by combining the moisture content and the horizontal velocity. IVT has

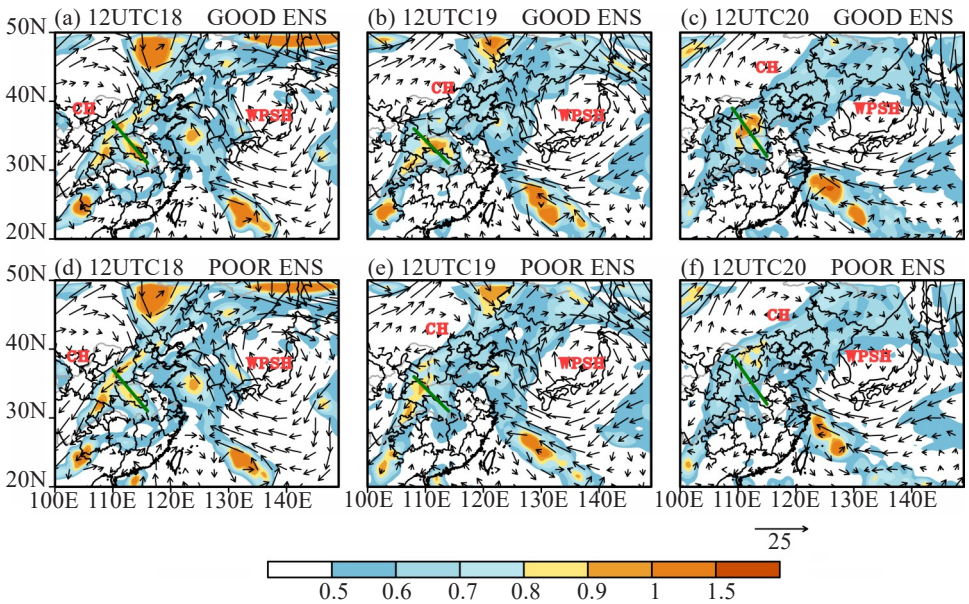

Figure 14. The time evolution of the PV (shaded, units: PVU; 1PVU=10^{-6} K m^2 s^{-1} kg^{-1}) and the wind circulation (units: m s^{-1}) for the two groups on 500-hPa (green lines: the cross sections of PV).

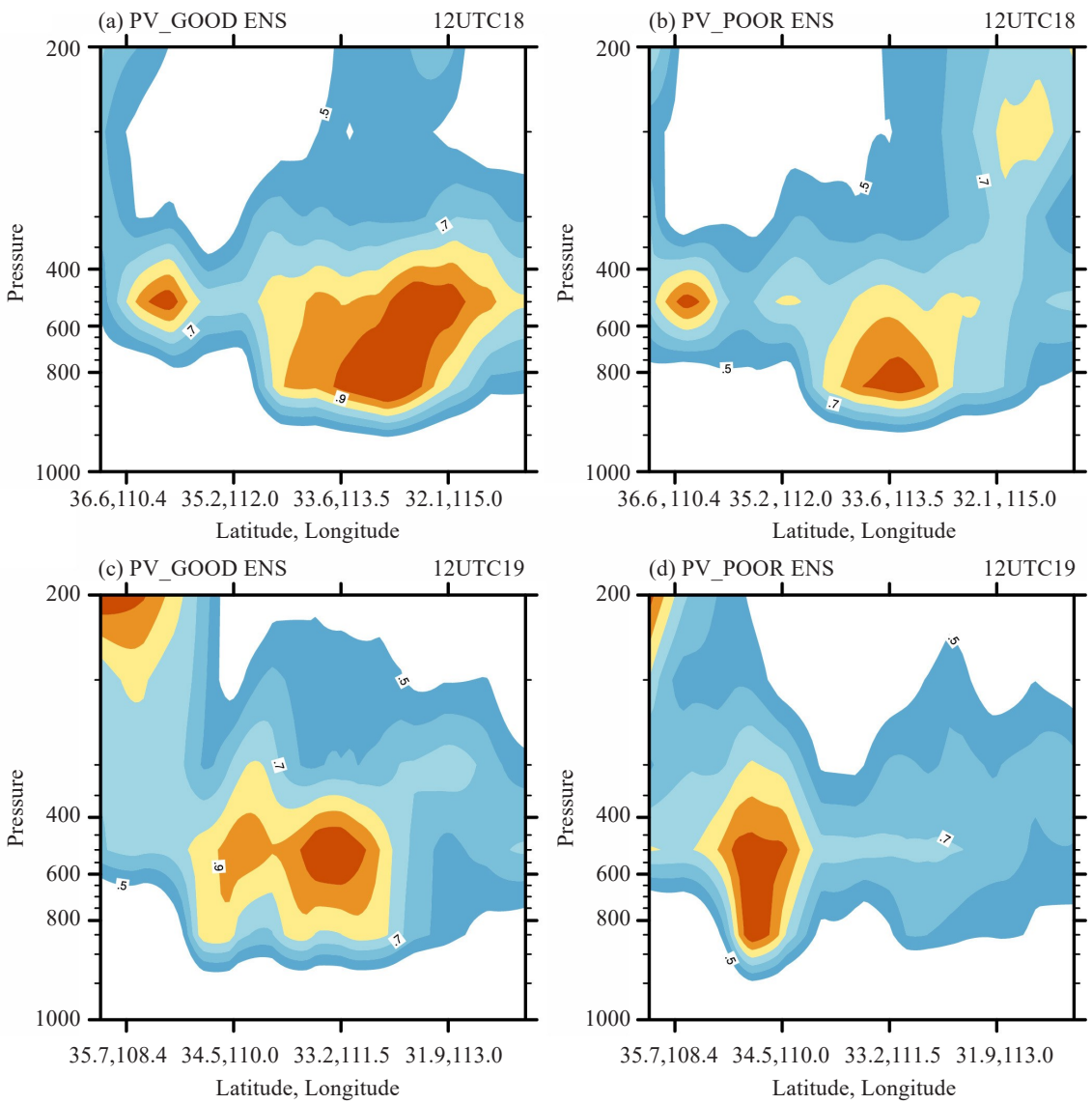

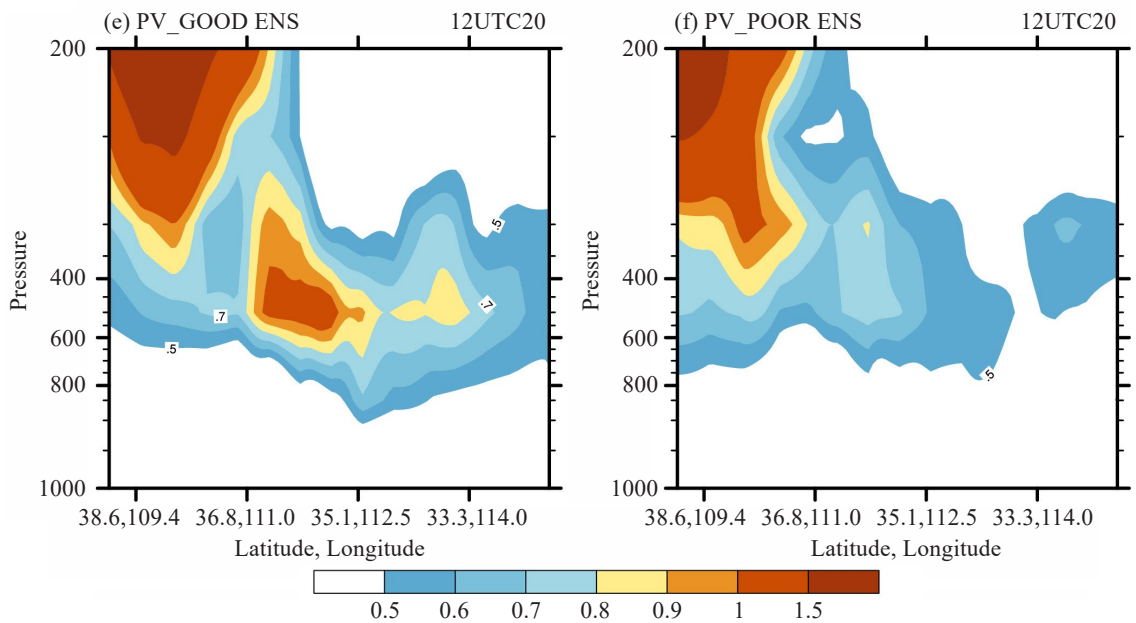

Figure 15. Vertical structure of the PV distributions (shaded, units: PVU; 1PVU=10^{-6} K m^2 s^{-1} kg^{-1}) along the direction perpendicular to the maximum PV for the two groups. The cross section is along the green lines in Fig. 14.

been used to characterize features of water vapor transport, which is defined as:

$$\mathrm{IVT}=\sqrt{\left(\frac{1}{g}\int_{P_0}^{P_{top}} qu\mathrm{d}p\right)^2+\left(\frac{1}{g}\int_{P_0}^{P_{top}} qv\mathrm{d}p\right)^2}, \qquad (4)$$

where u and v are the zonal and meridional wind speeds, q is the water vapor, and P_{top} and P_0 are the air pressure at the top and the bottom of the atmosphere.

Figure 16 presents the IVT averaged from 12 UTC 19 to 12 UTC 20 July in both groups. Clearly, there is a channel with large IVT, starting from the outer region of TC In-Fa. It is likely that, due to the existence of TC and WPSH, the enhanced easterly jet-like flows carry the moist air flow to the inland of China, fed into the YHV. The water vapor supply in Henan is conductive to the development of the heavy rainfall event. Furthermore, the IVT in the good group is larger than that in the poor group, particularly in Henan. For the negative value of GOOD-POOR in the area (120°–130° E, 28°–32° N), the difference is primarily ascribed to the different TC location (Fig. 13 a, c, and e). The mean TC position in POOR group is located more westward compared to that in GOOD. The value of GOOD-POOR in the area (120°–130° E, 28°–32° N) is negative (Fig. 16 c).

To further reveal the possible linkage between rainfall and IVT, Fig. 16(d) depicts the sensitivity of the 24-hour accumulated precipitation forecast to the IVT by the 50 ensemble members from ECMWF-EPS. It is speculated that this pattern is associated with wind speed and specific humidity. The larger the wind speed or water vapor, the higher the sensitivity value. Areas with high sensitivity surround the TC, indicating the major moisture source is associated with TC circulation. The precipitation is also sensitive to the moisture in Henan, indicating a high correlation between them. In addition to the large value of IVT sensitivity around TC circulation, the Pacific Ocean region where WPSH and TC circulation intersect and northeast China also show very large sensitivity (Fig. 16 d). A closer look at Fig. 16c shows that the regions with higher sensitivity value are collocated with the larger difference of IVT. The higher sensitivity value is ascribed to the differences in both circulation and moisture among the ensemble samples.

5 DISCUSSION AND CONCLUSIONS

An unprecedented heavy rainfall event occurred in Henan Province, China, during 19-20 July 2021 with a record of 522 mm accumulated rainfall (“21.7” event). In this study, the key controlling factors for the event and its predictability are examined. The sensitivity analysis of the precipitation forecasts is conducted using the ECMWF ensemble prediction system (EPS) to reveal the impacts of surrounding synoptic weather systems on the event. Among the 50 ensemble members, 21 members are selected based on their predicted maximum rainfall accumulations during the event and are divided into two groups. The Good group consists of 10 members with the maximum accumulated precipitation greater than 100 mm. There are 11 members in the POOR group with the maximum accumulated precipitation less than 50 mm.

The good members of the ECMWF-EPS are capable of capturing the spatial distribution of the heavy rainfall, but fail to predict its extremity. The comparisons between the good and poor members suggest the importance of accurate predictions of the evolution characteristics (i.e., intensity and location) of

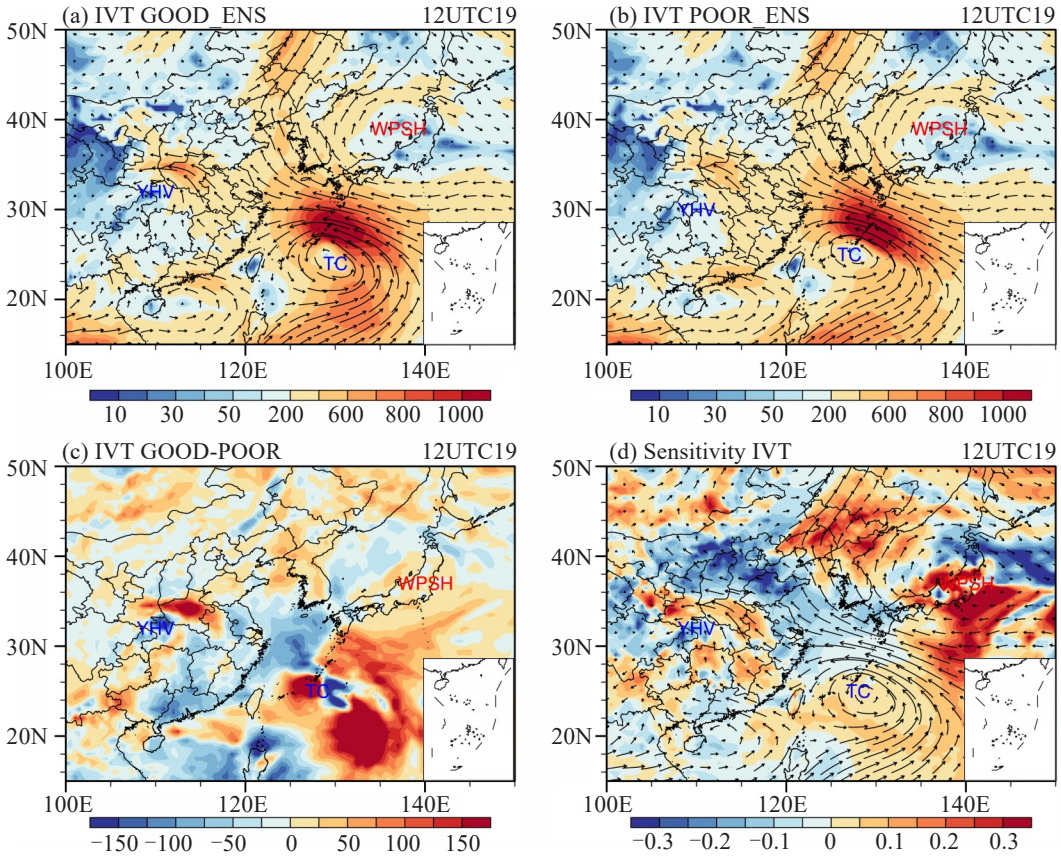

Figure 16. The IVT (shaded, units: kg $m^{-1}s^{-1}$) and the water vapor flux (vector, units: kg $m^{-1}s^{-1}$) of the two groups averaged from 12 UTC 19 July to 12 UTC 20 July. (a) the 10 good members; (b) the 11 poor members; (c) the difference between the good and poor members; (d) the sensitivity of the accumulated rain to the IVT and the water vapor flux of the ensemble mean (vector, units: kg $m^{-1}s^{-1}$) by the 50 ensemble members from ECMWF-EPS.

local Yellow-Huai River low vortex (YHV), tropical cyclone (TC) In-Fa and the western Pacific subtropical high (WPSH).

A schematic diagram, summarizing the findings of this study and showing significant weather systems affecting the rainfall event is presented in Fig. 17. The location of the heavy rainfall event is in Henan (represents by the symbol of blue cloud). During the period of interest, the YHV occurs in the center and south of Henan, and TC In-Fa is located in the northwest Pacific. Between the TC and the WPSH, the converging flow brings large moisture, feeds into the YHV and induces the perfect storm scenario. The cooperation among the systems (i. e., TC, WPSH and YHV) with their relative positions all have impacts on the rainfall event. The main findings are summarized as follows:

(1) The evolution features (i. e., the strength and location) of YHV play a crucial role in this extreme event. During its westward movement to the south of Henan, accompanying this is a relatively strong southerly wind in the southwestern region of Henan, which is convergent with the easterly flow channeled between TC In-Fa and the WPSH in the area adjacent to Zhengzhou City. The diagnoses also show that the better prediction is likely due to the dynamical processes involving multiple entities. These are conducive to the enhancements of surface convergence, resulting in a strong dynamical uplifting for heavy precipitation and high efficiency.

(2) The rainfall amount is highly sensitive to the prediction of TC In-Fa's location and intensity. Stronger TCs with a slower movement leads to heavier rainfall. Dynamically, the interactions between In-Fa and WPSH will induce an enhanced easterly flow, which acts as an atmospheric river to transport the abundant moisture to inland China, feeds into the YHV and causes heavy rainfall.

Admittedly, the ECMWF-EPS has large deviations in the prediction of the intensity and spatial distribution of heavy rainfall, especially lacks of its extremity. In addition to the initial error, the model error is one of error sources. For instance, the ESA cannot fully reflect the model errors such as the stochastic physical perturbation (SPPT) scheme. It is difficult to isolate this kind of model error, which awaits for future works. Furthermore, the model resolution is likely to be a key factor, since the global model cannot resolve the convective-scale systems, which are believed to play fundamental roles in this extreme event. For instance, the observed radar reflectively analysis shows that there

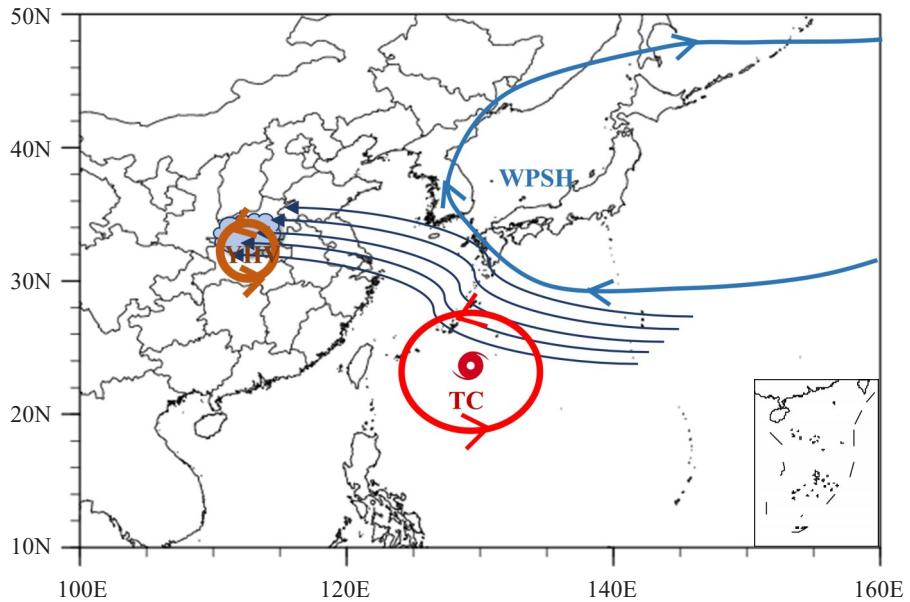

Figure 17. Schematic illustration of possible systems (i.e., YHV, TC and WPSH) that affect the rainfall event. The cloud mark is the region where the rainfall event occurred. Brown (Red) circle is the location of the YHV (TC). Blue semicircle represents the location of the WPSH. Dark blue arrows are the converging flows between the TC and the WPSH that bring large moisture into the northern China, fed into the YHV.

exist several multi-cell systems moving parallelly across the city, and the train effect cannot be captured in the ensemble prediction. Meanwhile, the cold pool dynamics of the rainfall event cannot be examined with the current dataset. Hence, we mainly focus on the synoptic-scale perspective. High-resolution convection-permitting ensemble will be conducted to investigate the local convective-scale and micro-scale processes in the future.

Acknowledgements: The numerical calculations are performed on the supercomputing system in the Supercomputing Center of Nanjing University of Information Science & Technology.

Data Availability Statement. All datasets used in this paper are publicly available. The observed precipitation data can be accessed at (https://data. cma. cn / data / cdcdetail/ dataCode / SURF_CLI_CHN_MUL_DAY_V3.0. html). The ECMWF ensemble Prediction data can be accessed at (https://apps. ecmwf.int/datasets/data/tigge/levtype=pl/type=cf/).

REFERENCES

[1] LUO Y L, WU M W, REN F M, et al. Synoptic situations of extreme hourly precipitation over China [J]. Journal of Climate, 2016, 29(24): 8703-8719, https://doi.org/10.1175/JCLI-D-16-0057.1

[2] CHEN L S, LUO Z. A preliminary study of the dynamics of eastward shifting cyclonic vortices [J]. Advances in Atmospheric Sciences, 2003, 20(3): 323-332, https://doi.org/10.1007/BF02690790

[3] LI N, RAN L K, GAO S T. The impact of deformation on vortex development in a baroclinic moist atmosphere [J]. Advances in Atmospheric Sciences, 2016, 33(2): 233-246, https://doi.org/10.1007/s00376-015-5082-y

[4] MADDOX R A, CHAPPELL C F, HOXIT L R. Synoptic and meso-α scale aspects of flash flood events [J]. Bulletin of the American Meteorological Society, 1979, 60(2): 115-123, https://doi.org/10.1175/1520-0477-60.2.115

[5] CHEN Y L, LI J. Large-scale conditions favorable for the development of heavy rainfall during TAMEX IOP 3 [J]. Monthly Weather Review, 1995, 123(10): 2978-3002, https: //doi. org / 10.1175 / 1520-0493(1995)123<2978: LSCFFT> 2.0.CO;2

[6] HOUZE R A, RUTLEDGE J S, BIGGERSTAFF M I, et al. Interpretation of Doppler weather radar displays of midlatitude mesoscale convective systems [J]. Bulletin of the American Meteorological Society, 1989, 70(6): 608-619.

[7] HOUZE R A. Mesoscale convective systems [J]. Reviews of Geophysics, 2004, 42(4): RG4003, https://doi. org / 10.1029/2004RG000150

[8] LAU K M, ZHOU Y P, WU H T. Have tropical cyclones been feeding more extreme rainfall? [J]. Journal of Geophysical Research: Atmospheres, 2008, 113(D23): D23113, https://doi.org/10.1029/2008JD009963

[9] ZHANG D L, LIN Y, ZHAO P, et al. The Beijing extreme rainfall of 21 July 2012: "Right results" but for wrong reasons [J]. Geophysical Research Letters, 2013, 40(7): 1426-1431, https://doi.org/10.1002/grl.50304

[10] IWASAKI H. Increasing trends in heavy rain during the warm season in eastern Japan and its relation to moisture variation and topographic convergence [J]. International Journal of Climatology, 2015, 35(8): 2154-2163, https://doi.org/10.1002/joc.4115

[11] LUO Y L, GONG Y, ZHANG D L. Initiation and organizational modes of an extreme-rain-producing mesoscale convective system along a Mei-Yu front in East China [J]. Monthly Weather Review, 2014, 142(1):

203-221, https://doi.org/10.1175/MWR-D-13-00111.1
[12] LUO Y L, CHEN Y R X. Investigation of the predictability and physical mechanisms of an extreme-rainfall-producing mesoscale convective system along the Meiyu front in East China: An ensemble approach [J]. Journal of Geophysical Research: Atmospheres, 2015, 120 (20): 10593-10618, https://doi. org / 10.1002 / 2015JD023584
[13] LUO Y L, SUN J S, LI Y, et al. Science and prediction of heavy rainfall over China: Research progress since the reform and opening-up of new China [J]. Journal of Meteorological Research, 2020, 34(3): 427-459, http://jmr.cmsjournal.net/article/doi/10.1007/s13351-020-0006-x
[14] WANG Y Q, WANG Y Q, FUDEYASU H. The role of Typhoon Songda (2004) in producing distantly located heavy rainfall in Japan [J]. Monthly Weather Review, 2009, 137(11): 3699-3716, https://doi. org / 10.1175 / 2009MWR2933.1
[15] CONG C H, LEI X T, CHEN P Y, et al. A comparative study on two processes of typhoon remote rainfall over Shandong Province [J]. Periodical of Ocean University of China (in Chinese), 2016, 46(12): 21-31, https://doi.org/10.16441/j.cnki.hdxb.20160034
[16] WU C C, CHEUNG K K W, LO Y Y. Numerical study of the rainfall event due to the interaction of typhoon Babs (1998) and the Northeasterly Monsoon [J]. Monthly Weather Review, 2009, 137(7): 2049-2064, https://doi.org/10.1175/2009MWR2757.1
[17] LUO Y, ZHANG L F. A case study of the error growth evolution in a Meiyu front heavy precipitation forecast and analysis of the predictability [J]. Acta Meteorologica Sinica (in Chinese), 2010, 68(3): 411-420.
[18] ZHOU F F, CUI X P. The adjoint sensitivity of heavy rainfall to initial conditions in debris flow areas in China [J]. Atmospheric Science Letters, 2015, 16(4): 485-491, https://doi.org/10.1002/asl.586
[19] ANCELL B, HAKIM G J. Comparing adjoint and ensemble sensitivity analysis with applications to observation targeting [J]. Monthly Weather Review, 2007, 135(12): 4117-4134, https://doi. org / 10.1175 / 2007MWR1904.1
[20] HAKIM G J, TORN R D. Ensemble Synoptic Analysis [M]// BOSART L F, BLUESTEIN H B (eds), Synoptic—Dynamic Meteorology and Weather Analysis and Forecasting. Boston: American Meteorological Society, 2008: 147-161.
[21] TORN R D, HAKIM G J. Initial condition sensitivity of Western-Pacific extratropical transitions determined using ensemble-based sensitivity analysis [J]. Monthly Weather Review, 2009, 137(10): 3388-3406, https:/doi. org / 10.1175/2009MWR2879.1
[22] BROWN B R, HAKIM G J. Sensitivity of intensifying Atlantic hurricanes to vortex structure [J]. Quarterly Journal of the Royal Meteorological Society, 2015, 141 (692): 2538-2551, https://doi.org/10.1002/qj.2540
[23] MATSUEDA M, KYOUDA M, TOTH Z, et al. Predictability of an atmospheric blocking event that occurred on 15 December 2005 [J]. Monthly Weather Review, 2011, 139(8): 2455-2470, https://doi.org/10.1175/2010MWR3551.1
[24] QUANDT L A, KELLER J H, MARTIUS Q, et al. Ensemble sensitivity analysis of the blocking system over Russia in summer 2010 [J]. Monthly Weather Review, 2009, 147(2): 657-675, https://doi.org/10.1175/MWR-D-18-0252.1
[25] TORN R D. Ensemble-based sensitivity analysis applied to African easterly waves [J]. Weather and Forecasting, 2010, 25(1): 61-78, https://doi. org/ 10.1175 / 2009WAF2222255.1
[26] HILL A J, WEISS C C, ANCELL B C. Ensemble sensitivity analysis for mesoscale forecasts of dryline convection initiation [J]. Monthly Weather Review, 2016, 144(11): 4161-4182, https://doi.org/10.1175/MWR-D-15-0338.1
[27] LIMPERT G L, HOUSTON A L. Ensemble sensitivity analysis for targeted observations of supercell thunderstorms [J]. Monthly Weather Review, 2018, 146 (6): 1705-1721, https://doi. org / 10.1175 / MWR-D-17-0029.1
[28] YU H Z, MENG Z Y. Key synoptic-scale features influencing the high impact heavy rainfall in Beijing China on 21 July 2012 [J]. Tellus A: Dynamic Meteorology and Oceanography, 2016, 68(1): 31045, https://doi.org/10.3402/tellusa.v68.31045
[29] DU Y, CHEN G X. Heavy rainfall associated with double low-level jets over Southern China, Part I : ensemble-based analysis [J]. Monthly Weather Review, 2018, 146 (11): 3827-3844, https://doi. org / 10.1175 / MWR-D-18-0101.1
[30] WU N G, ZHUANG X R, MIN J Z, et al. Practical and intrinsic predictability of a warm-sector torrential rainfall event in the South China monsoon region [J]. Journal of Geophysical Research: Atmospheres, 2020, 125: e2019JD031313, https://doi.org/10.1029/2019JD031313
[31] RAN L K, LI S W, ZHOU Y S, et al. Observational analysis of the dynamic, thermal, and water vapor characteristics of the "7.20" extreme rainstorm event in Henan Province [J]. Chinese Journal of Atmospheric Sciences (in Chinese), 2021, 45(6): 1366－1383, https://doi.org/10.3878/j.issn.1006-9895.2109.21160
[32] SHI W R, LI X, ZENG M J, et al. Multi-model comparison and high-resolution regional model forecast analysis for the "7·20" Zhengzhou severe heavy rain [J]. Transactions of Atmospheric Sciences (in Chinese), 2021, 44(5): 688 － 702, https://doi. org / 10.13878 / j. cnki. dqkxxb.20210823001
[33] SUN Y, XIAO H, YANG H L, et al. Analysis of dynamic conditions and hydrometeor transport of Zhengzhou superheavy rainfall event on 20 July 2021 based on optical flow field of remote sensing data [J]. Chinese Journal of Atmospheric Sciences (in Chinese), 2021, 45 (6): 1384－1399, https://doi. org / 10.3878 / j. issn. 1006-9895.2109.21155
[34] ZHANG X, YANG H, WANG X M, et al. Analysis on characteristic and abnormality of atmospheric circulations of the July 2021 extreme precipitation in Henan [J]. Transactions of Atmospheric Sciences (in Chinese), 2021, 44(5): 672 － 687, https://doi. org / 10.13878 / j. cnki. dqkxxb.20210907001
[35] TORN R D, HAKIM G J. Ensemble-based sensitivity analysis [J]. Monthly Weather Review, 2008, 136(2): 663-677, https://doi.org/10.1175/2007MWR2132.1
[36] YANG G M, MAO D Y, YAO X P. The analysis of dry intrusion feature of a Huanghuai cyclone development in

Meiyu period [J]. Journal of Tropical Meteorology (in Chinese), 2006, 22(2): 176-183, https://doi.org/10.16032/j.issn.1004-4965.2006.02.010

[37] QIAN W H, LI J, SHAN X. Application of synoptic-scale anomalous winds predicted by medium-range weather forecast models on the regional heavy rainfall in China in 2010 [J]. Science China Earth Sciences, 2013, 56: 1059-1070, https://doi.org/10.1007/s11430-013-4586-5

[38] OKUBO A. Horizontal dispersion of floatable particles in the vicinity of velocity singularities such as convergences [J]. Deep Sea Research and Oceanographic Abstracts, 1979, 17(3): 445-454, https://doi.org/10.1016/0011-7471(70)90059-8

[39] WEISS J. The dynamics of enstrophy transfer in two-dimensional hydrodynamics [J]. Physica D: Nonlinear Phenomena, 1991, 48(2-3): 273-294, https://doi. org / 10.1016/0167-2789(91)90088-Q

[40] ZHANG F Q, DAVIS C A, KAPLAN M L, et al. Wavelet analysis and the governing dynamics of a large-amplitude mesoscale gravity-wave event along the East Coast of the United States [J]. Quarterly Journal of the Royal Meteorological Society, 2001, 127(577): 2209-2245, https://doi.org/10.1002/qj.49712757702

[41] KOCH S E, DORIAN P B. A mesoscale gravity wave event observed during CCOPE, Part III: Wave environment and probable source mechanisms [J]. Monthly Weather Review, 1988, 116(12): 2570-2592, https://doi. org / 10.1175 / 1520-0493(1988)116<2570:AMGWEO>2.0.CO;2

[42] XU H X, XU X D, ZHANG S J, et al. Long-range moisture alteration of a typhoon and its impact on Beijing extreme rainfall [J]. Chinese Journal of Atmospheric Sciences (in Chinese), 2014, 38(3): 537-550, https://doi.org/10.3878/j.issn.1006-9895.2013.13173

[43] LU H C, ZHONG W, ZHANG D L. Current understanding of wave characteristics in tropical storm [J]. Chinese Journal of Atmospheric Sciences (in Chinese), 2007, 31(6): 1140-1150, https://doi.org/10.3878/j.issn.1006-9895.2007.06.10

[44] ROSSBY C G. Planetary flow patterns in the atmosphere [J]. Quarterly Journal of the Royal Meteorological Society, 1940, 66: 68-87.

[45] ERTEL H. Ein neuer hydrodynamischer Wirbelsatz [J]. Meteorology Zeitschr (in German), 1942, 59: 272-281.

[46] DOSWELL III C A, BROOKS H E, MADDOX R A. Flash flood forecasting: An ingredients-based methodology [J]. Weather and Forecasting, 1996, 11(4): 560-581, https://doi.org/10.1175/1520-0434(1996)0112.0.CO;2

[47] ZHU Y, NEWELL R E. A proposed algorithm for moisture fluxes from atmospheric rivers [J]. Monthly Weather Review, 1998, 126(3): 725-735, https://doi. org/10.1175/1520-0493(1998)126<0725:APAFMF>2.0.CO;2

Citation: HUANG Qi-jun, GE Xu-yang, PENG Melinda, et al. Sensitivity Analysis of the Super Heavy Rainfall Event in Henan on 20 July (2021) Using ECMWF Ensemble Forecasts [J]. Journal of Tropical Meteorology, 2022, 28(3): 308-325, https://doi. org/10.46267/j.1006-8775.2022.024